Analysis of Video-Based Microscopic Particle Trajectories Using Kalman Filtering

Pei-Hsun Wu,[†] Ashutosh Agarwal,[‡] Henry Hess,[¶] Pramod P. Khargonekar,[§] and Yiider Tseng[†‖*]
[†]Department of Chemical Engineering, [‡]Department of Materials Science and Engineering, and [§]Department of Electric and Computer Engineering, University of Florida, Gainesville, Florida; [¶]Department of Biomedical Engineering, Columbia University, New York, New York; and [‖]National Cancer Institute-Physical Science in Oncology Center, Gainesville, Florida

ABSTRACT The fidelity of the trajectories obtained from video-based particle tracking determines the success of a variety of biophysical techniques, including in situ single cell particle tracking and in vitro motility assays. However, the image acquisition process is complicated by system noise, which causes positioning error in the trajectories derived from image analysis. Here, we explore the possibility of reducing the positioning error by the application of a Kalman filter, a powerful algorithm to estimate the state of a linear dynamic system from noisy measurements. We show that the optimal Kalman filter parameters can be determined in an appropriate experimental setting, and that the Kalman filter can markedly reduce the positioning error while retaining the intrinsic fluctuations of the dynamic process. We believe the Kalman filter can potentially serve as a powerful tool to infer a trajectory of ultra-high fidelity from noisy images, revealing the details of dynamic cellular processes.

INTRODUCTION

The motion of intracellular particles, such as macromolecular complexes or organelles, is crucial for the spatial and temporal organization of cell function (1,2). Bacterial invasion into mammalian cells also involves harnessing the ability of the microorganism to move within the intracellular microenvironment of host cells (3). High-resolution imaging is the most direct method of studying the physical motion of intracellular objects and tracked particles. For example, the video analysis of motor protein-driven transport of particles has greatly improved our understanding of the function of motor proteins (4,5). In these studies, particle tracking served as the fundamental method for studying the real-time movement of the transported objects in living cells.

Particle tracking has been applied successfully to study various subcellular events, such as genomic dynamics (6), viral infection (7,8), cellular endocytosis (9), membrane protein trafficking (10), and cargo transport (11). Particle tracking has also been applied to probe the mechanical properties of the intracellular region of the live cells via particle tracking microrheology (12), which analyzes the displacement fluctuations of an inert particle embedded in the cytoplasmic region of a live cell. Using the microrheology theorem (13,14), the rheological parameters of a cell, such as creep compliance, elastic modulus, and viscous modulus, have been quantified (12,15). Compared to other techniques, such as atomic force microscopy, intracellular microrheology acquires the physical properties of the intracellular region of the cells with minimal perturbations. Using this technique, the mechanical properties of various cell lines under different extracellular stimuli (chemical (15) and mechanical (16)) and microenvironmental topology (two-dimensional versus three-dimensional (17)) have been probed.

Because the particle-tracking technique can contribute valuable insights into many biological events, the accuracy of particle tracking is critically important for effectiveness of those studies. However, in a particle tracking experiment, the sensor noise in the image acquisition system is transformed into a positioning error. As a result, the computed particle trajectory is a noisy version of the true particle trajectory. This hinders a deeper analysis of the trajectory aimed at gaining detailed insights into the dynamic process related to the observed object (Fig. 1) (18). Accordingly, many advanced instruments were recently developed, which improve the spatial resolution of tracking techniques (19,20). However, signal filtering and estimation algorithms offer an alternative route to reducing the extraneous noise associated with particle trajectories. These algorithms can be applied regardless of the underlying instrumentation, and thus provide a general approach that can effectively enhance the spatial resolution of particle tracking.

Deriving states of a dynamic system from noisy measurements is a very well-researched problem in control and estimation theory. In particular, the Kalman filter (21) algorithm provides the optimal state estimate for linear dynamic systems from sensor measurements in the presence of Gaussian noise. The Kalman filter is a technique and has been successfully applied in a wide variety of situations in engineering and science (22,23). The potential to use a Kalman filter to study cell motion has been mentioned in passing (24). In this study, we explore in detail the

Submitted December 29, 2009, and accepted for publication March 10, 2010.

*Correspondence: ytseng@che.ufl.edu

Abbreviations used: ACF, autocorrelation function; fps, frames per second; MSD, mean-square displacement; Q, variance of thermal fluctuation; Q_T, true variance of thermal fluctuation; R, variance of positioning error; RMSE, root mean-square errors; R_T, true variance of positioning error.

Editor: Xiaowei Zhuang.

0006-3495/10/06/2822/9 $2.00

doi: 10.1016/j.bpj.2010.03.020

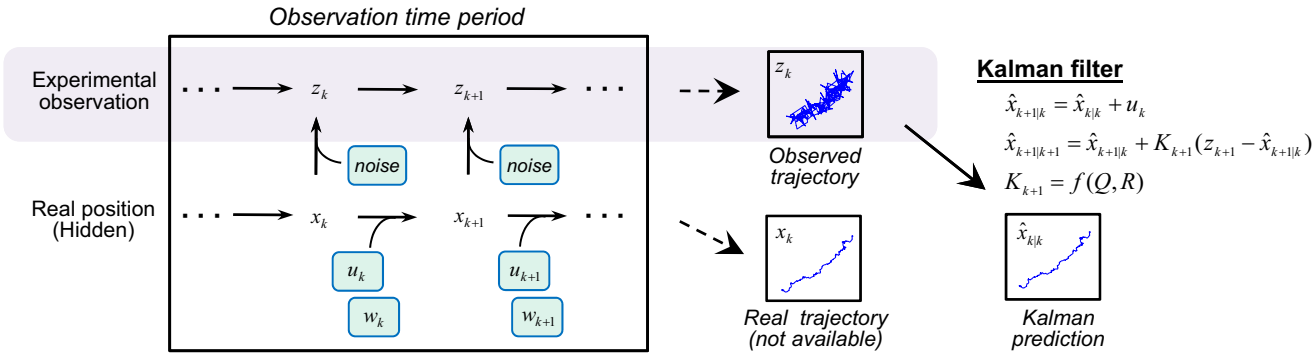

FIGURE 1 Schematic illustration of the principle of Kalman filter in estimating the accurate trajectory in a cellular dynamic process. The relation between adjacent steps of a trajectory is $x_{k+1} = x_k + u_k + w_k$, where the occurring displacements before the next monitored time for the particle in x_k position are determined by its projective movement displacement, u_k, and a random movement generated by thermal fluctuation, w_k. The subscript k represents the k^{th} step of the tracking trajectory. In tracking experiments, the real particle position, x_{k+1}, is recorded as z_{k+1} due to the positioning error. The Kalman filter is an established algorithm to restore the correct trajectory for a linear process.

application of the Kalman filter algorithm to improve the estimation of the particle trajectory obtained from a microscopic particle tracking experiment.

We first show that the Kalman filter can be used to estimate the intrinsic trajectories from noisy measurements. Next, we explain how the input parameters (the variance of process and measurement noise) necessary for the design of the Kalman filter can be estimated for a given experimental situation. Third, we discuss the efficacy of the Kalman filter in particle tracking. Finally, we examine in vitro particle tracking in glycerol and in a gliding motility assay to validate the application of the Kalman filter. We conclude that the Kalman filter can effectively eliminate the positioning error generated by measurement noise if the measurement noise and process fluctuation variance parameters are chosen appropriately. As a result, the accuracy of the trajectory derived from particle tracking experiments is improved, which in turn can provide the reliable biophysical information critical for the understanding of various biological processes.

MATERIALS AND METHODS

The parameters of the Kalman filter related to a particle tracking trajectory

Video-based particle tracking uses the visual information in a sequence of captured images to reconstruct the trajectories of labeled objects and determine their dynamical properties. The temporal resolution in a particle tracking experiment is determined from the time between each frame, represented by Δt. Individual image frames in the tracking sequence can then be denoted by their respective timestep, k, and a subscript k can represent the value of a given variable at time $k \times \Delta t$. Conceptually, the position of a tracked object in a new frame at time $(k + 1) \times \Delta t$ is the result of a combination of active motion and random displacements due to thermal fluctuations that acted on the object over Δt because its previous position at time $k \times \Delta t$. In biological systems, the heterogeneous presence of obstacles restricts the magnitude of an object's velocity in a manner that intrinsically fluctuates. Thus, the change in position between timesteps can be described by a constant directed movement, u_0, associated with a fluctuation, w_0, as well as the intrinsic thermal fluctuations. Using an ensemble fluctuation term, w_k, to account for w_0 and the thermal fluctuations, the conceptual position, x_{k+1}, of a tracked object in a new frame can be formulated as:

$$x_{k+1} = x_k + u_0 + w_k. \quad (1)$$

This relationship between position, active motion, and thermal fluctuations has been established previously in different forms (25,26). However, during the image acquisition process there is an intrinsic measurement noise, v_k, that leads to the measured position, z_k, from its true value x_k as described by:

$$z_k = x_k + v_k. \quad (2)$$

The Kalman filter is a recursive, computational method to make an estimate of the true value of the position x_k from the knowledge of the noisy observations z_k (while preserving their intrinsic fluctuations (21)). However, having a better understanding of the parameters that govern the motion of an object is necessary before describing the major input factors of the Kalman filter. The measurement noise, v_k, is assumed to obey:

$$v_k \sim N(0, R_k), \quad (3)$$

where $N(0,R_k)$ is the Gaussian distribution function describing white noise with a zero mean and a variance of position measurement error, R_k. Similarly, the process noise w_k caused by thermal fluctuations is assumed to obey:

$$w_k \sim N(0, Q_k), \quad (4)$$

where $N(0,Q_k)$ is also the Gaussian distribution function with zero mean and variance of thermal fluctuations, Q_k. In one-dimensional Brownian dynamics, $Q_k = 2 \times D \times \tau$, where D is the effective diffusivity of a labeled object and τ is the diffusion time. If tracking object undergoes pure Brownian motion, the value of u_0 is zero, and the value of w_k only represents the thermal fluctuations. In the case of directed motion, the magnitude of u_0 can be experimentally estimated by calculating the average displacement between timesteps, i.e., $u_0 = \langle z_{k+1} - z_k \rangle$. We will assume that Q_k and R_k are time-invariant, i.e., independent of k, and denote them by Q and R respectively.

Taking all of this into account, the most important parameters of the Kalman filter are the raw trajectory information and the variance terms Q and R. The value of R for a tracked particle can be extracted as described previously (27), but the value of Q must be attained using another method. The MSD of the measured trajectory, z_k, is calculated as the variance of the measured displacement, $S(\equiv \mathrm{var}(dz))$, and is related to Q and R by (18,27):

$$S = Q + 2 \times R. \quad (5)$$

Because noise from image acquisition does not directly influence the physical system of interest, the value of Q is independent of R, and this relationship serves as an explicit method to estimate Q.

The Kalman filter gain is determined by the ratio Q/R but not Q or R

$$K = \frac{(Q/R) + \sqrt{(Q/R)^2 + 4(Q/R)}}{2 + (Q/R) + \sqrt{(Q/R)^2 + 4(Q/R)}}. \quad (6)$$

The Kalman filter gain (or Kalman gain) is the key parameter than governs the filter algorithm and determines the performance of the Kalman filter. The computation of K is carried out by applying the standard Kalman filtering theory that leads to the optimal value of K under assumptions of linear dynamics with Gaussian process and measurement noise. The analytical relationship of the Kalman gain to the ratio Q/R is determined as Eq. 6 (see Supporting Material). This equation underscores the fact that for our model (Eqs. 1–4) the value of K depends on the Q/R but not the individual Q- and R-values.

Application of the Kalman filter to simulated trajectories

The trajectory of a labeled object undergoing linear motion (e.g., Brownian motion or active movement containing thermal fluctuation) can be simulated based on Eq. 1 and Eq. 4. The effective diffusivity and temporal resolution applied to the simulation were 0.006 $\mu m^2/s$ and 0.033 s, respectively, which were extracted from particle tracking experiments of 100-nm microspheres in glycerol solution. From these conditions, the variance of a one-dimensional thermal fluctuation is represented by Q_T (= 2 × 0.006 × 0.033). For the simulation of Brownian motion the velocity of active movement is set to zero. In each simulation, a trajectory contains 1000 timesteps; and extrinsic noise with variance, R_T, is further added to each step based on Eq. 2 and Eq. 3 to mimic the positioning error resulting from the imaging process.

The Kalman filter was then applied to these simulated noisy trajectories using several values of Q and R to understand the performance of the filter as the input variance terms differed from their true values (here, Q_T and R_T). The accuracy of the filtered trajectory was evaluated by calculating the RMSE (i.e., $\sqrt{(\hat{x}_{k|k} - x_k)^2}$).

Microscopic particle tracking system

A Cascade:1K EMCCD camera (Roper Scientific, Tucson, AZ) mounted on a TE 2000-E inverted microscope (Nikon, Melville, NY) with a 60×, NA 1.45, oil-immersion objective lens (Nikon) was used to acquire particle-tracking video for image analysis. The particle tracking experiments were carried out by capturing video at a rate of 30 fps. Each image sequence is composed of 650 frames. To achieve this high temporal resolution, the region of interest function in the camera was activated and the binning was set at 3-by-3 for the particle tracking in glycerol (390 nm effective pixel size) and 2-by-2 for the gliding motility assay (260 nm effective pixel size).

Particle tracking experiments in glycerol solutions

Carboxylated polystyrene fluorospheres (Invitrogen, Carlsbad, CA) with 100-nm diameter in water were diluted into glycerol at 1:1000 volume ratio. A drop of the mixture was placed on the central area of a glass bottom dish (MatTek, Ashland, MA) for video-based particle tracking experiments. The particle tracking method was described previously (27). In brief, the background noise of the raw image stack was reduced using a Gaussian kernel filter (18,28). Afterward, a two-dimensional Gaussian distribution with logarithmic weighting was used to least-square fit the intensity distribution of the particles in the region contains the pixel possessing the maximum intensity and its four adjacent pixels to determine the positions of the particles.

Particle tracking experiments in gliding motility assays

Kinesin was prepared as described previously (29). Microtubules were prepared by polymerizing 20 μg biotin-labeled tubulin (Cytoskeleton, Denver, CO) in 6.5 μL growth solution, containing 4 mM $MgCl_2$, 1 mM GTP, and 5% (v/v) DMSO in BRB80 buffer (80 mM PIPES, pH 6.9, 1 mM $MgCl_2$, 1 mM EGTA) for 30 min at 37°C. The microtubules were 100-fold diluted and stabilized in 10 μM Paclitaxel (Sigma, St. Louis, MO). The experiments were carried out in ~100 μm high and 1 cm wide flow cells assembled from two coverslips and double-stick tape (30). First, BRB80 with 0.5 mg/mL casein (Sigma) was injected into the flow cell. After 5 min, it was exchanged with a kinesin solution (BRB80 with 0.5 mg/mL casein, ~10 nM kinesin, and 20 μM ATP). Five minutes later, this was exchanged against a motility solution (0.2 mg/mL casein, 20 mM D-glucose, 20 μg/mL glucose oxidase, 8 μg/mL catalase, 10 mM dithiothreitol, and 20 μM ATP in BRB80) containing 0.8 μg/mL biotinylated microtubules. Five minutes were allowed for microtubule attachment after which 20 nM Alexa 568-labeled streptavidin (Invitrogen) in motility solution was perfused into the flow cell and incubated for 5 min to cover all the biotin sites on the microtubules (31). Finally, after three washes with motility solution, biotin-labeled 40 nm fluorospheres (Invitrogen) at 100 pM concentration in motility solution were introduced into the flow cell and the edges of the flow cell were sealed with Apiezon grease to minimize evaporation.

RESULTS

To explore the application of the Kalman filter to effectively correct the influence of measurement noise on position estimation in single particle-tracking experiments, an error-free Brownian trajectory was simulated to serve as the reference trajectory (Fig. 2 *A*). Positioning errors with increasing variance values, denoted as R, were individually added to the reference trajectory to derive four noisy trajectories (Fig. 2 *B*; from the left to the right, R = 0.0004, 0.0011, 0.004, and 0.04, respectively). In these simulated trajectories, the input parameters, including the R-values, were chosen based on typical experimental conditions (27). The Kalman filter was applied to these trajectories and the root mean-square errors (RMSE) of the positions between the estimated trajectories and the error-free trajectory were determined. The application of the Kalman filter requires two input parameters, the variance of thermal fluctuation (Q) (from process noise) and the variance of positioning error (R) (from measurement noise), which are not known a priori. We first chose identical values for Q and R and calculated the resulting RMSE values to determine whether Kalman filtering could improve the noisy trajectories. The results show that the Kalman filter can reduce the positioning error even if the input parameters are arbitrarily assigned (Fig. 2 *C*). However, if the true values of Q and R are used

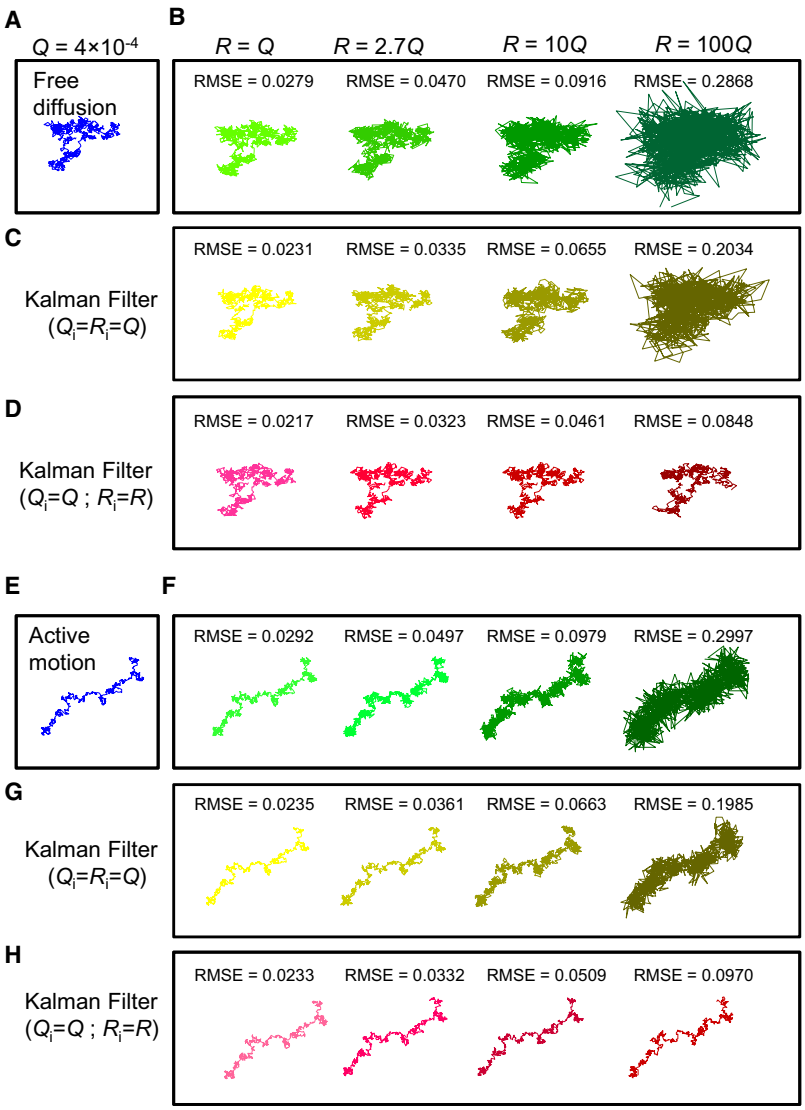

FIGURE 2 Estimation of the true trajectory from positioning errors using Kalman filter. (*A*) A simulated Brownian motion trajectory is represented without positioning error. (*B*) Increasing degrees (from left to right) of positioning error (quantified by its variance R) are added to the simulated trajectory. Higher R-values yield noisier trajectories. (*C*) The Kalman filter removes some extrinsic noise under an arbitrary setting of the input parameters R_i and Q_i, e.g., $Q_i = R_i = Q$, where Q is the thermal fluctuation variance. (*D*) The Kalman filter restores the noisy trajectories if the correct Q- and R-value are used as input parameters Q_i and R_i. (*E*) A simulated active motion trajectory is represented without positioning error. (*F*) Increasing degrees of positioning error are added to the active motion trajectory. (*G*) The Kalman filter improves the noisy trajectories under the setting $Q = R$. (*H*) The Kalman filter restores the noisy trajectories under the correct Q and R setting.

(known for the simulation), the positioning error of the noisy trajectories can be further reduced up to ~3-fold (Fig. 2 *D*).

The evaluation of the Kalman filter was further extended to trajectories describing active motion. Active motion trajectories without (Fig. 2 *E*) or with positioning error (Fig. 2 *F*; from the left to the right, $R = 0.0004$, 0.0011, 0.004, and 0.04, respectively) were simulated. Either arbitrary (Fig. 2 *G*) or accurate (Fig. 2 *H*) Kalman filter input parameters were applied to the noisy trajectories to estimate the true trajectories. Again, the positioning error generated during the acquisition process was reduced, and the optimal performance of the Kalman filter depended on the correct choice of input parameters.

These simulations suggest that the Kalman filter can effectively eliminate positioning error caused by measurement noise while retaining the intrinsic thermal fluctuations if the input parameters, Q and R, are available. However, the Q and R are two independent unknowns, whose values cannot be directly determined from an acquired image. Previously, we developed a Monte Carlo method that uses empirical parameters obtained from images to extract the value of R (27). This value of R is a positioning error that is individually estimated for each of our imaging experiments because R depends strongly on the incident light intensity and parameters of the acquisition system. The value of Q can be determined using Eq. 5 (18,27). Because S can be obtained from experiments, the value of Q can be obtained as $S - 2 \times R$ (Fig. 3; also see Materials and Methods). A potential shortcoming of this method is that errors in the determination of R and S directly affect the accuracy of Q.

To assess the impact of inaccurate Q- and R-values in a model system, we tracked freely diffusive 100-nm diameter carboxylated polystyrene fluorescent particles in glycerol at room temperature and an acquisition frequency of 33 fps. These experiments were repeated many times and the value

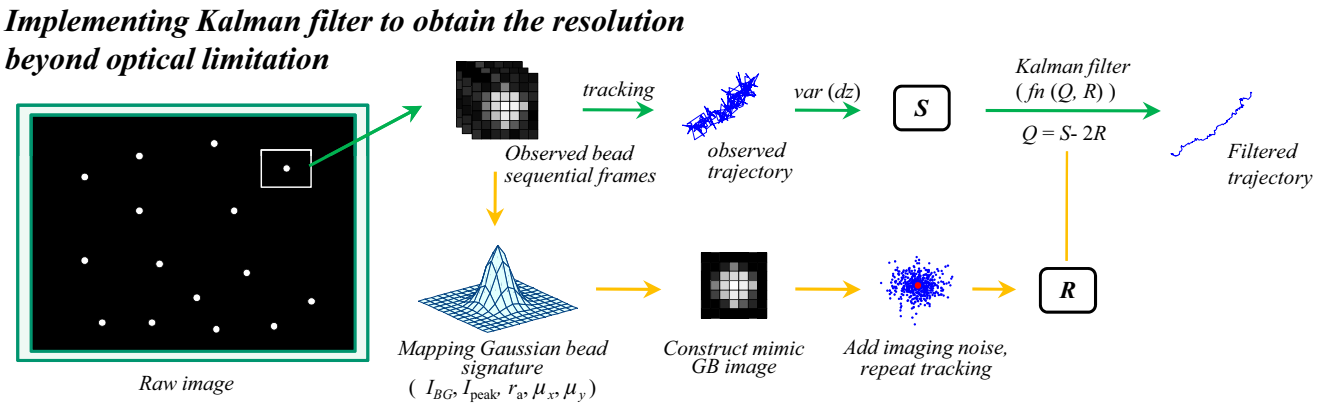

FIGURE 3 Schematic illustration of the procedure of implementing Kalman filter into a microscopic particle tracking system to improve the spatial resolution The acquired images are used to extract the parameters to simulate Gaussian particle, which is applied to the particle-tracking algorithm to determine the variance of positioning error (R). The R-value and corresponding Q-value, determining by the MSD of the tracking trajectory and R-value, then be used as the input parameters for Kalman filter to restore the true trajectory.

of R was estimated using the Monte Carlo procedure for each experiment (27). Comparing the resulting microrheological measurement of the viscosity of glycerol with a conventional rheological measurement validated the accuracy of R. The standard deviation (SD) of R from 20 independent simulations is <3%, which is a further indication of the precision of this technique. Next, S was calculated as the MSD of the particles, and the value of Q for each experiment was obtained by using the relation, $Q_i = S_i - 2 \times R_i$, where the subscript i represents an independent tracking experiment. A plot of S and Q against the corresponding R shows that S and R are proportional to each other whereas Q remains constant through different values of R (Fig. 4 *A inset*). This calculated Q-value was also in agreement with the theoretically calculated thermal fluctuations at room temperature, Q_{RT} ($= 0.8 \times 10^{-3}$ μm^2) (27). We next determined the mean and the SD of Q within fixed intervals of R (Fig. 4 *A*). Although Q and R are independent, the SD of Q does increase with R. Because the experimental values of Q and R can be obtained, we can evaluate the performance of the Kalman filter on measured trajectories using the experimentally determined Q and R.

For the linear dynamic model, it is easily shown that the Kalman gain is determined only by the ratio of Q to R, and not the individual Q- and R-values (see Eq. 6 and Supporting Material). Thus, we described the performance of Kalman

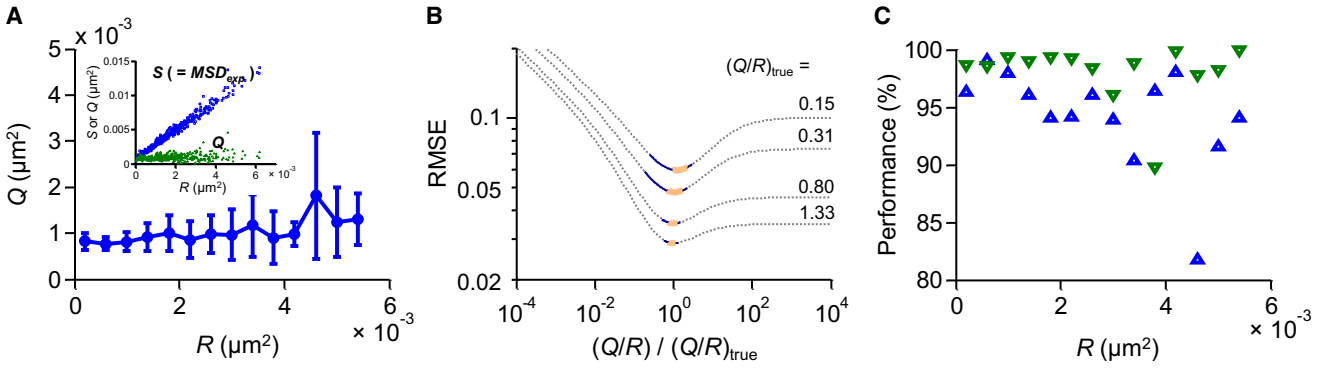

FIGURE 4 Characterization of the performance of Kalman filter on estimating particle tracking trajectories. (*A*) The variance of thermal fluctuation (Q) can be extracted from the variance of displacement (S) and the variance of positioning error (R) using the relationship, $Q = S - 2 \times R$. The mean of Q is estimated for different intervals of R, with an interval size of 0.4×10^{-3} μm^2. The error bar represents the SD of Q. The resolution of Q decreases with increasing of R. (*Inset*) The trajectories contain 504 data points from particle tracking in glycerol described in the methods section. (*B*) Kalman filter performance is determined by the accurate Q/R value. Using the experimental R-values and their corresponding ranges of Q-value in simulations, the RMSE of the Kalman filter-estimating trajectories, compared to the simulated true trajectory, can be obtained. The light (*orange*) and dark (*blue*) region represents the RMSE value for Q-value within one or two SDs of the mean. (*C*) The performance of the Kalman filter in estimating the true trajectory measured by the RMSE reduction relative to the maximal RMSE reduction achieved for $Q/R = (Q/R)_T$. At the minimal RMSE value, the estimating trajectory carries a MSD value equal to the true trajectory (see Supporting Material). The filtered trajectory is identical to the unfiltered trajectory if there is no positioning error ($R = 0$) or if no improvement has been achieved that occurs in for very large normalized Q/R. Thus, the RMSE value at large Q/R represents the original RMSE value of the tracked trajectory. The maximum improvement of the RMSE value thus is equal to the difference between the RMSE value at large Q/R and the minimal RMSE value in the RMSE-Q/R curve.

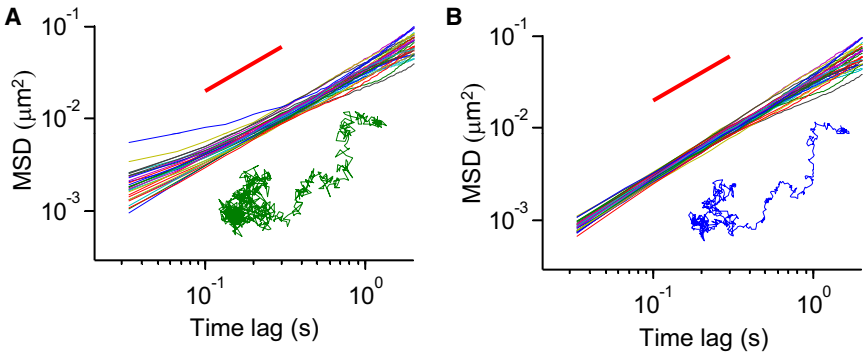

FIGURE 5 Improving the positioning error of particle tracking in glycerol solution using Kalman filter. (*A*) The MSD curves were obtained by particle tracking of 100-nm carboxylated polystyrene fluorescent microspheres in glycerol, 31 microspheres were tracked. (*B*) The MSD curves were calculated from the filtered trajectories. (*Insets*) One of the trajectories (*A*) before and (*B*) after application of the Kalman filter.

filtering by the plot of RMSE versus normalized Q/R ($= (Q/R)/(Q_T/R_T) = (Q/R)/(Q/R)_T$), where the Q_T and R_T represent the true variances of thermal fluctuation and positioning error in the acquired image, respectively (Fig. 4 *B*). As expected, the minimum RMSE value always occurs at normalized $Q/R = 1$, where the Kalman filter uses the accurate input ratio for the parameters, Q and R. Because the determination of the Q-value using the procedure described above has some uncertainty (*light orange* region: 1 SD around mean of Q; *dark blue* region: 2 SD around the mean), the RMSE values obtained using the experimentally determined Q/R tend to be slightly larger than the optimum. These RMSE values can be compared to the RMSE value at very large normalized Q/R (e.g., 10^4). In this region, the Kalman filter assumes minimal measurement noise and places a much greater reliance on the measurements by making minimal changes to the measured trajectory. Therefore, the RMSE values at very large normalized Q/R are representative of the unfiltered RMSE values. A comparison shows that the experimentally obtained R- and Q-values lead the Kalman filter to estimate more accurate trajectories with smaller RMSE values when compared to the RMSE values of the original trajectory.

Based on the experimental data, we can quantify the percentage of RMSE improvement after applying the Kalman filter (Fig. 4 *C*). Using the mean value of R in each R-interval and the corresponding Q at the mean $\pm$ 1 SD as the input parameters of the Kalman filter, the RMSE of the filtered trajectories can be calculated and compared to the minimal RMSE value obtained for Q/R equal to $(Q/R)_T$. The data ((▼) left- and (▲) right-bound in Fig. 4 *C*) suggests that within the SD (68.2%) of the Q-value, the Kalman filter achieves at least 82% of the maximal reduction in RMSE value. First, considering that an accurate estimate of R can be obtained in the experiment using our Monte Carlo simulation technique, second, that the estimate of Q/R determined in real experiments has a limited range (e.g., normalized Q/R values vary from ~0.79 to 1.16 and ~0.63 to 2.3 for $R \sim 6 \times 10^{-4}$ and 3.4×10^{-3} μm^2, respectively, in Fig. 4 *B*), and finally that the filtered RMSE value for input parameters, Q and R, in this limited range is very close to the minimum RMSE value obtained for the optimal Q/R, we conclude that the application of Kalman filter as described can reliably reduce the positioning error generated in the image acquisition process.

To show the application of the Kalman filter to experimental data of a purely diffusive process, particle tracking of 100-nm carboxylated polystyrene fluorescent microspheres in glycerol was carried out and the MSD profiles (Fig. 5 *A*) were calculated from the tracking trajectories (a representative trajectory was shown in Fig. 5 *A*, *inset*). When the Kalman filter was applied to these trajectories using the values of R and Q extracted from the tracking images, a group of new MSD profiles (Fig. 5 *B*) can be calculated from the filtered trajectories (a filtered trajectory is shown in Fig. 5 *B*, *inset*). Because glycerol is a homogenous solution and the MSD profiles generated from the trajectories of the diffusing microspheres should overlap, the narrowing of the bundle of MSD profiles shows the removal of extrinsic noise by the Kalman filter. The more accurate determination of the intrinsic MSD using the Kalman filter enables a better resolution of molecular processes in subcellular dynamics studies.

We further applied the Kalman filter to an active transport process by estimating a more accurate trajectory of beads attached to a microtubule gliding on surface-adhered kinesin-1 motors (Fig. 6 *A*). These position data and the extracted parameters, R and Q, from the images were used as input for the Kalman filter, and the estimated trajectory for the microtubule was obtained (Fig. 6 *B*). The average distance covered as a function of the time between frames (Fig. 6 *C*) and the variance of the fluctuations around this average distance as a function of the time lag (Fig. 6 *D*) show the expected linear behavior (24,32,33) for the filtered trajectory, whereas system noise distorts the unfiltered quantities. If the microtubules were stationary objects, the position variance of the attached beads would not display this linear increase. However, the active movement of the microtubules during the gliding motility assays will directly affect the observed position of the attached beads. In essence, the gliding motion is thought to consist of a movement with constant velocity (caused by the active transport by the surface-adhered motors) superimposed with a diffusive movement against a high drag caused by protein friction (motor binding events that do not contribute a forward force). Thus, it is the diffusive movement of the microtubules and not the attached

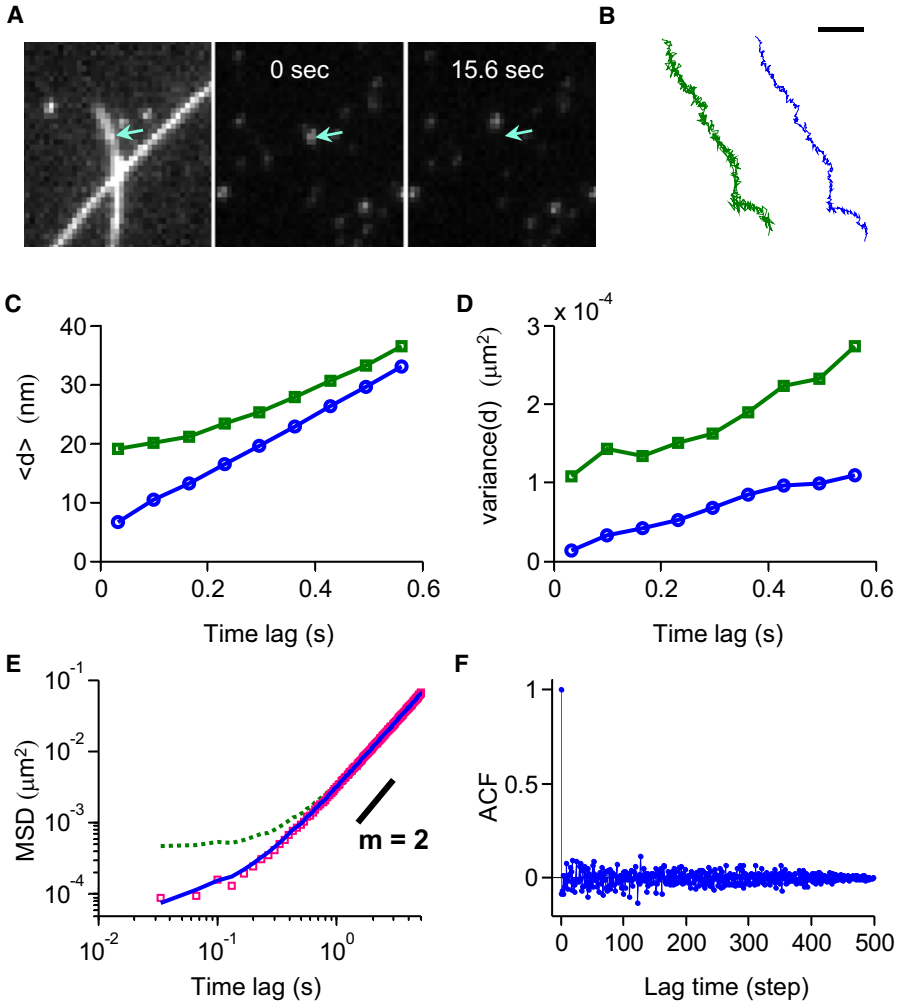

FIGURE 6 Improving the positioning error of particle tracking in gliding motility assays using Kalman filter. (*A*) Images of a gliding motility assay. Images from left to right represent the microtubule, the nanosphere at 0 s and the nanosphere at time 15.6 s, respectively. The arrow indicates the initial position of the nanosphere, which is moving with a microtubule. (*B*) Observed trajectory (*left*) and filtered trajectory (*right*) of this nanosphere during the observation time period (15.6 s). Scale bar = 200 nm. (*C*) Average of nanosphere displacement as a function of time interval. Removal of noise reduces the displacement at small time intervals of the filtered trajectory (○) relative to the raw trajectory (□), as expected for movement with constant velocity. (*D*) Variance of nanosphere displacement as a function of time interval for the filtered (○) and raw (□) trajectory. Removal of measurement noise yields the expected linear function starting at the origin and enables a correct estimate of the motional diffusion coefficient (24). (*E*) MSD from the different particle trajectories for different time lag is plotted. The value of the observed MSD (*dashed line*) is roughly fivefold higher in comparison to MSD values with static error removed (*solid line*) and MSD values calculated from the Kalman filtered trajectory (□). (*F*) The innovation residual of the Kalman filter ($z_k - \hat{x}_k$ or the difference between observed and predicted positions) is theoretically Gaussian white noise. The ACF of innovation residual is plotted against different time lag. Accordingly, the ACF is independent of lag time, which is a feature of Gaussian white noise.

beads that causes the linearly increasing positional variance of the beads. Previous studies of gliding cytoskeletal filaments, such as actin filaments and microtubules, have also interpreted the increasing positional variance as a result of protein friction (24,34–39).

The glycerol and in vitro gliding motility studies show that the Kalman filter can restore particle trajectories from diffusive as well as active transport, providing a more accurate picture of the underlying dynamics. To further verify the results from the motility studies, an independent method to correct for trajectory error was carried out and compared to the Kalman filtered MSD values and the raw data. The MSD profiles from the two different methods shared an approximate fivefold decrease in MSD value from the raw data and were in good agreement when directly overlaid (Fig. 6 *E*). Another way to verify the success of Kalman filtering is to analyze the ACF of the innovation sequence ($z_k - \hat{x}_k$; measured position − predicted position) of the Kalman filter. Theoretically, assuming correctness of the model the innovation sequence is Gaussian white noise. In this case, its ACF will be nonzero at zero lag and be zero for all other time lags. We have plotted this in Fig. 6 *F* (40) and it can be seen that the innovation sequence is white. Through these separate analyses of the Kalman filtering of the gliding motility assay, which are independent of the stochastic model used, we can solidly conclude that the Kalman filter can be successfully applied to this in vitro system.

DISCUSSION

In summary, the purpose for this study was to introduce the application of the Kalman filter to the biological field as a first step to explore this type of direction. The Kalman filter has evolved since its initial development into an extremely powerful tool in many applications, even including successful application to the stock market (21). However, the current involvement of the Kalman filter in biology is limited, and this work suggests that the intracellular Kalman filtering approach is feasible with careful progress based on the investigation of the in vitro systems studied here.

The application of the Kalman filter to biological systems will encounter several challenges that must be overcome. Subcellular dynamics are often complicated and effective models that can faithfully describe them are usually

unavailable. Many factors, such as the thermal fluctuations, the steric effects from heterogeneous cellular architecture and the dynamics of the cytoskeleton reorganization, contribute to the complexity of the dynamic movement of a micron- or submicron-scaled tracer inside a living cell. Therefore, the first step to using a Kalman filter for this type of approach is to determine the appropriate stochastic model describing the motion of a subcellular object. Such a model would highly depend on several factors describing the intracellular objects of interest such as diffusivity, cell cycle stage, microenvironmental conditions and composition. As the model is developed, it can be incorporated into a Kalman filter using the same methodology as the in vitro systems discussed in this work. With the correct stochastic model in place, the Kalman filter could become a powerful tool to reduce measurement noise and reveal the real-time dynamic interactions between a particle and its microenvironment.

Another challenge facing the application of the Kalman filter to intracellular dynamics is the presence of photobleaching effects or big movements out of the focal plane in particle tracking experiments. For typical particles like quantum dots and 100-nm diameter fluorescence microspheres, which possess Q/R values within the range studied here, the variance of the positioning error (R) is assumed to be unchanged during the observation period in our in vitro studies. However, these conditions may not be fulfilled when studying the dynamics of a single molecule in living cells at 30 fps due to the large mobility of the probing molecule. The reported diffusivity of GFP in cytoplasm is 20 $\mu m^2/s$ and the focal depth ~1 μm. Thus, the time required for the GFP to diffuse out of the focal plane is ~0.05 s ($\sim L^2/D$). In that case, the R-value would be a function of the molecular position in the z-direction and change markedly if the temporal resolution is not correspondingly >30 fps. Photobleaching effects would also change the R-value because the dimming of particles lowers their peak intensity, causing a gradual increase in positioning error. As the temporal resolution is increased to offset movements out of the focal plane, the acquired images would be correspondingly dimmer unless the light source intensity was increased, which would further irritate photobleaching problems.

This trade-off between temporal and spatial resolution has limited our ability to further explore the cellular dynamic process of subcellular components and intracellular microrheology (41,42). Video-based microscopy studies have provided a qualitative understanding of this issue (43), but an optimal balance of temporal and spatial resolution has not yet been developed fully. Recent developments in photon detection techniques allow us to track object movement with high temporal resolution (44), which would help to compensate for movements out of the focal plane. As these types of techniques develop and a more comprehensive knowledge of spatio-temporal resolution emerges, problems associated with photobleaching effects and movements out of the focal plane can be overcome. High temporal resolution could then be used in a particle tracking experiment at the expense of some degree of spatial resolution that could later be restored analytically by proper use of the Kalman filter, increasing our capacity to identify and quantitatively characterize subtle intracellular motion.

In this study, we characterized the performance of the Kalman filter in estimating the native trajectory of particles diffusing within a glycerol solution and the transport process of microtubules in vitro. As the difficulties that naturally arise in the particle tracking of intracellular dynamics are resolved, this study can provide a guideline to carefully judge the performance of the Kalman filter in new biological applications. We showed that the Kalman filter is an effective tool to eliminate positioning error incorporated into the real trajectory during image acquisition while preserving the inherent thermal fluctuations, and that the success of the Kalman filter depends on the correct setting for the parameter describing Q/R. Kalman filtering can preserve the native fluctuations while removing the measurement noise; hence it greatly enhances the reliability of an estimated trajectory.

In our previous study (27), we have shown that the value of R in a particle tracking experiment can be extracted using a Monte Carlo simulation technique. The extracted value of R is highly reproducible and successfully corrects the static error of noisy MSD curves. In this study, we have further shown that by using the values of Q and R extracted from experiments, the individual trajectory resulting from the Kalman filter is optimized. The reliability of Kalman filter in predicting the trajectory can be assessed by the RMSE computation, which is compared to a simulated, true trajectory. The trajectory estimation from the Kalman filter using the extracted values of Q and R can lead to a significant reduction of the RMSE value, close to the minimal value achievable with exact knowledge of Q and R. At this minimum, the estimated trajectory carries a MSD equal to the MSD obtained from the true trajectory that can be proved mathematically as well (see Supporting Material). Therefore, we conclude that Kalman filter can effectively improve the video-based particle-tracking trajectory in the in vitro systems we have examined.

SUPPORTING MATERIAL

Two figures are available at http://www.biophysj.org/biophysj/supplemental/S0006-3495(10)00352-8.

The authors are grateful for Dr. M. Ding and Dr. T. Lele for their thoughtful discussion.

This research was partially funded by National Institutes of Health (U54CA143868 and R01EB004416).

REFERENCES

1. Detmer, S. A., and D. C. Chan. 2007. Functions and dysfunctions of mitochondrial dynamics. *Nat. Rev. Mol. Cell Biol.* 8:870–879.

2. Saftig, P., and J. Klumperman. 2009. Lysosome biogenesis and lysosomal membrane proteins: trafficking meets function. *Nat. Rev. Mol. Cell Biol.* 10:623–635.
3. Goldberg, M. B., and J. A. Theriot. 1995. *Shigella flexneri* surface protein IcsA is sufficient to direct actin-based motility. *Proc. Natl. Acad. Sci. USA.* 92:6572–6576.
4. Hua, W., E. C. Young, …, J. Gelles. 1997. Coupling of kinesin steps to ATP hydrolysis. *Nature.* 388:390–393.
5. Kural, C., H. Kim, …, P. R. Selvin. 2005. Kinesin and dynein move a peroxisome in vivo: a tug-of-war or coordinated movement? *Science.* 308:1469–1472.
6. Levi, V., Q. Ruan, …, E. Gratton. 2005. Chromatin dynamics in interphase cells revealed by tracking in a two-photon excitation microscope. *Biophys. J.* 89:4275–4285.
7. van der Schaar, H. M., M. J. Rust, …, J. M. Smit. 2007. Characterization of the early events in dengue virus cell entry by biochemical assays and single-virus tracking. *J. Virol.* 81:12019–12028.
8. Brandenburg, B., and X. Zhuang. 2007. Virus trafficking—learning from single-virus tracking. *Nat. Rev. Microbiol.* 5:197–208.
9. Ruan, G., A. Agrawal, …, S. Nie. 2007. Imaging and tracking of tat peptide-conjugated quantum dots in living cells: new insights into nanoparticle uptake, intracellular transport, and vesicle shedding. *J. Am. Chem. Soc.* 129:14759–14766.
10. Wieser, S., M. Moertelmaier, …, G. J. Schütz. 2007. (Un)confined diffusion of CD59 in the plasma membrane determined by high-resolution single molecule microscopy. *Biophys. J.* 92:3719–3728.
11. Salman, H., A. Abu-Arish, …, M. Elbaum. 2005. Nuclear localization signal peptides induce molecular delivery along microtubules. *Biophys. J.* 89:2134–2145.
12. Tseng, Y., T. P. Kole, and D. Wirtz. 2002. Micromechanical mapping of live cells by multiple-particle-tracking microrheology. *Biophys. J.* 83:3162–3176.
13. Mason, T. G., K. Ganesan, …, S. C. Kuo. 1997. Particle tracking microrheology of complex fluids. *Phys. Rev. Lett.* 79:3282–3285.
14. Apgar, J., Y. Tseng, …, D. Wirtz. 2000. Multiple-particle tracking measurements of heterogeneities in solutions of actin filaments and actin bundles. *Biophys. J.* 79:1095–1106.
15. Kole, T. P., Y. Tseng, …, D. Wirtz. 2004. Rho kinase regulates the intracellular micromechanical response of adherent cells to rho activation. *Mol. Biol. Cell.* 15:3475–3484.
16. Lee, J. S., P. Panorchan, …, D. Wirtz. 2006. Ballistic intracellular nanorheology reveals ROCK-hard cytoplasmic stiffening response to fluid flow. *J. Cell Sci.* 119:1760–1768.
17. Panorchan, P., J. S. Lee, …, D. Wirtz. 2006. Microrheology and ROCK signaling of human endothelial cells embedded in a 3D matrix. *Biophys. J.* 91:3499–3507.
18. Savin, T., and P. S. Doyle. 2005. Static and dynamic errors in particle tracking microrheology. *Biophys. J.* 88:623–638.
19. Yildiz, A., M. Tomishige, …, P. R. Selvin. 2004. Kinesin walks hand-over-hand. *Science.* 303:676–678.
20. Unruh, J. R., and E. Gratton. 2008. Analysis of molecular concentration and brightness from fluorescence fluctuation data with an electron multiplied CCD camera. *Biophys. J.* 95:5385–5398.
21. Kalman, R. E. 1960. A new approach to linear filtering and prediction problems. *J. Basic Eng.* 82:35–45.
22. Zarchan, P., and H. Musoff. 2009. Fundamentals of Kalman Filtering: A Practical Approach. American Institute of Aeronautics and Astronautics, Reston, VA.
23. Ramachandra, K. 2000. Kalman Filtering Techniques for Radar Tracking. Marcel Dekker, New York, NY.
24. Ionides, E. L., K. S. Fang, …, G. F. Oster. 2004. Stochastic models for cell motion and taxis. *J. Math. Biol.* 48:23–37.
25. Imafuku, Y., Y. Y. Toyoshima, and K. Tawada. 1996. Fluctuation in the microtubule sliding movement driven by kinesin in vitro. *Biophys. J.* 70:878–886.
26. Gibbons, F., J. F. Chauwin, …, J. V. José. 2001. A dynamical model of kinesin-microtubule motility assays. *Biophys. J.* 80:2515–2526.
27. Wu, P. H., S. H. Arce, …, Y. Tseng. 2009. A novel approach to high accuracy of video-based microrheology. *Biophys. J.* 96:5103–5111.
28. Gonzalez, R. C., and R. E. Woods. 2002. Digital Image Processing. Prentice Hall, Upper Saddle River, NJ.
29. Coy, D. L., M. Wagenbach, and J. Howard. 1999. Kinesin takes one 8-nm step for each ATP that it hydrolyzes. *J. Biol. Chem.* 274: 3667–3671.
30. Howard, J., A. J. Hunt, and S. Baek. 1993. Assay of microtubule movement driven by single kinesin molecules. *Methods Cell Biol.* 39:137–147.
31. Ramachandran, S., K. H. Ernst, …, H. Hess. 2006. Selective loading of kinesin-powered molecular shuttles with protein cargo and its application to biosensing. *Small.* 2:330–334.
32. Leduc, C., F. Ruhnow, …, S. Diez. 2007. Detection of fractional steps in cargo movement by the collective operation of kinesin-1 motors. *Proc. Natl. Acad. Sci. USA.* 104:10847–10852.
33. Nitta, T., and H. Hess. 2005. Dispersion in active transport by kinesin-powered molecular shuttles. *Nano Lett.* 5:1337–1342.
34. Tawada, K., and K. Sekimoto. 1991. Protein friction exerted by motor enzymes through a weak-binding interaction. *J. Theor. Biol.* 150:193–200.
35. Tawada, K., and K. Sekimoto. 1991. A physical model of ATP-induced actin-myosin movement in vitro. *Biophys. J.* 59:343–356.
36. Sekimoto, K., and K. Tawada. 1995. Extended time correlation of in vitro motility by motor protein. *Phys. Rev. Lett.* 75:180–183.
37. Imafuku, Y., Y. Y. Toyoshima, and K. Tawada. 1996. Monte Carlo study for fluctuation analysis of the in vitro motility driven by protein motors. *Biophys. Chem.* 59:139–153.
38. Imafuku, Y., Y. Emoto, and K. Tawada. 1999. A protein friction model of the actin sliding movement generated by myosin in mixtures of MgATP and MgGTP in vitro. *J. Theor. Biol.* 199:359–370.
39. Sekimoto, K., and K. Tawada. 2001. Fluctuations in sliding motion generated by independent and random actions of protein motors. *Biophys. Chem.* 89:95–99.
40. Stengel, R. F. 1986. Stochastic Optimal Control: Theory and Application. Wiley, New York, NY.
41. Kole, T. P., Y. Tseng, …, D. Wirtz. 2005. Intracellular mechanics of migrating fibroblasts. *Mol. Biol. Cell.* 16:328–338.
42. Lee, J. S., C. M. Hale, …, D. Wirtz. 2007. Nuclear lamin A/C deficiency induces defects in cell mechanics, polarization, and migration. *Biophys. J.* 93:2542–2552.
43. Jaqaman, K., and G. Danuser. 2009. Computational image analysis of cellular dynamics: a case study based on particle tracking. *CSH Protoc.* 2009:top65.
44. McMahon, M. D., A. J. Berglund, …, J. A. Liddle. 2009. 3D particle trajectories observed by orthogonal tracking microscopy. *ACS Nano.* 3:609–614.